

# Saturation effects on two- and three-dimensional digital holographic reconstructions employing a CCD camera

Alejandro Salazar Lobos, ID: 1517982<sup>1,\*</sup>

<sup>1</sup>Department of Physics, University of Alberta, Edmonton, AB, Canada T6G 2G7

Digital numerical holographic reconstruction by discrete Fresnel transformation was performed successfully on surfaces: a CAD dime and a US dime. It was found that the quality of the reconstruction of the surface depended on the complexity of its high relief pattern and on the saturation of the CCD camera used to record the holograms. Reconstruction of the surface is based on phase information of the electric field of light, and when just enough saturation of the CCD was achieved, so that phase information was not distorted, it was observed that a more complex surface gave reconstructions of better quality. Conclusions about what determines the quality of a three-dimensional reconstruction are not definitive, but it is speculated that a successful tomography heavily depends on the type of wavefront hitting the CCD, with a planar front expected to give better results.

## I. INTRODUCTION

Digital holography consists in the discrete recording, digital storage, and numerical reconstruction of wavefronts.[4] The path for the beginning of digital holography in the 1990s required the invention of highly coherent light, or a laser [4]; a method to avoid spherical aberration, invented by Dennis Gabor in 1948 [2]; and electronic sensors, such as CCD and CMOS cameras [2], that were able to record wavefront information as holograms.[2, 4] Despite its relatively young age, digital holography has found its way to applications in microscopy, 3D imaging, data storage, and information processing.[4] Other applications include particle analysis [1] and fluid flow analysis. The reverse process is also being explored. With the use of spatial light modulators as hologram planes, researchers aim at being able to reconstruct three-dimensional wave fields. This would allow for the reconstruction of virtual 3D moving scenes.[1]

This report focused on the exploration of the effects of light saturation of a CCD camera on the quality of static holographic reconstructions. Specifically, exploration of the two-dimensional reconstruction of surfaces using coins, and an initial exploration of tomographic, or three-dimensional, reconstructions are offered. The reconstructions here are limited to small objects, of about the size of a dime for surfaces, and of about the thickness of a hair for 3D reconstructions. This makes the results presented here suitable for further investigation of the application of digital holography in information storage and in 3D imaging microscopy, for example.

## II. THEORY

We consider a source of light whose wavefront hits an obstacle. We think of the obstacle as an infinitely thin transparent surface that has opaque structures embedded in it. When the size of these structures are comparable to the size of the light wavelength, then, on the other side of the aperture, we see a diffraction pattern according to Huygens' principle, which says that every point in a wavefront acts as a source point of secondary wavefronts that interfere with each other.[6] (See

Figure 1.)

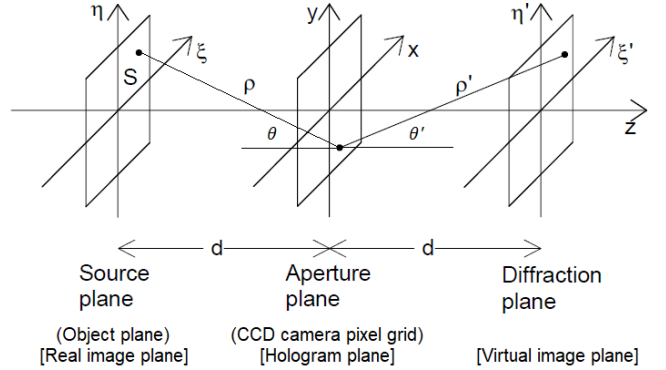


FIG. 1: Coordinate system. Adapted from Figure 2.5, p. 17, in Schnars & Jueptner (2005).

If the aperture plane is such that it records intensity and phase information about the field coming from the source of light, then we call it a hologram plane. In the context of this experiment, the hologram plane is the pixel grid of a CCD camera; we think of the pixels as the opaque structures that record information of diffraction. A source of light, in this experiment a reflective object, is placed in the source (or object) plane. In digital holography, for infinitely small pixels, the information of the field at the source plane is described by the Fresnel-Kirchhoff integral (refer to Figure 1 for the coordinate system) [6]:

$$\Gamma(\xi, \eta) = \frac{i}{\lambda} \int_a^b \int_a^b h(x, y) g_{PSF}(x - \xi, y - \eta) Q dx dy, \quad (1)$$

where  $\lambda$  is the light wavelength, and which says that the field at the source plane is proportional to the field at the aperture/CCD,  $h(x, y)$ , and the field of the secondary wavelets generated from diffraction exciting the aperture/CCD,  $g_{PSF}$ . The transformation of information from the aperture plane to the source plane is accomplished by the point spread function [5, 6]:

$$g_{PSF} = \frac{\exp(-i \frac{2\pi}{\lambda} \rho)}{\rho}, \quad (2)$$

$$\rho = \sqrt{(x - \xi)^2 + (y - \eta)^2 + d^2},$$

\*Electronic address: [aasalaza@ualberta.ca](mailto:aasalaza@ualberta.ca)

where  $\rho$  is the distance between corresponding points in the source plane and hologram plane.

In this experiment, the distance between the CCD camera and the object was much larger than the dimensions of the pixel grid and the object, so we can Taylor-expand the point spread function.  $Q = \frac{1}{2}(\theta - \theta')$  in Equation (1) is a correction to Huygens' principle; it forces the propagation of light to occur in only one direction. Since  $d \gg$  "dimensions of pixel grid and object",  $\theta \approx \theta' \approx 0$ , and so  $Q \approx 1$ . In addition, the pixels had a definite size and formed an  $N \times N$  grid, so Equation 1 must be discretised. These modifications turn Equation (1) into [6]:

$$\begin{aligned} \Gamma(\xi, \eta) = & \frac{i}{\lambda} \exp(-i \frac{2\pi}{\lambda} d) \exp(-i\pi\lambda d[(\frac{m}{N\Delta x})^2 + (\frac{n}{N\Delta y})^2]) \\ & \times \sum_{k=0}^{N-1} \sum_{l=0}^{N-1} h(x, y) \exp(-i \frac{pi}{\lambda d} [(k\Delta x)^2 + (l\Delta y)^2]) \\ & \exp(i2\pi(\frac{km}{N} + \frac{ln}{N})), \\ m = & 0, 1, 2, \dots, N-1; n = 0, 1, 2, \dots, N-1, \end{aligned} \quad (3)$$

which is called the Fresnel transformation; it is a Fourier inverse transform of the function  $h(x, y) \exp(-i \frac{pi}{\lambda d} [(k\Delta x)^2 + (l\Delta y)^2])$  [6], and it is the formula used to perform numerical reconstructions of the holograms recorded by the CCD camera. Basically, it brings information of the object's image in Fourier/hologram space back to real space; this is the principle of holographic reconstruction. In this experiment, two types of holographic reconstructions are explored: 2D holographic reconstruction of a surface with a high relief pattern and the tomographic reconstruction of a three-dimensional object.<sup>endnote1</sup>

### III. EXPERIMENTAL DETAILS

Figure 2 shows the setup used for 2D holographic reconstructions. An He-Ne laser class IIIB of wavelength 635nm was used. Its beam was expanded through a beam expander, and then it went through a first 50/50 beam splitter. Half of the light (object beam) hit the object and was reflected off it onto a Lumera Lw575C CCD camera pixel grid. The other half, the reference beam, was reflected off a mirror, passed through a neutral density filter and finally, redirected towards the CCD camera through a second 50/50 beam splitter, where it recombined with the object beam. The CCD camera had a  $2592 \times 1944$ ,  $2.2\mu\text{m}$  square pixels. The captured profiles were cropped to  $1944 \times 1944$  pixels for reconstruction.

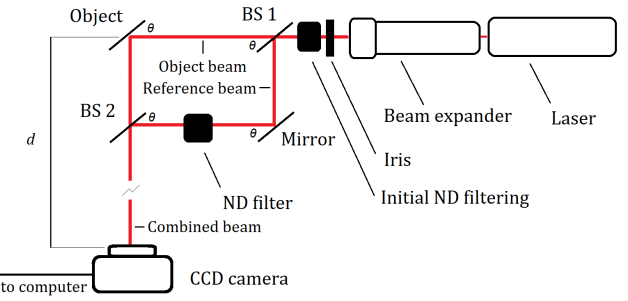


FIG. 2: Setup for 2D holographic reconstructions: BS is for "beam splitter", and ND, for "neutral density".  $d = 0.45\text{m}$  is the distance between the object and the CCD.  $\theta = 45^\circ$ .

The neutral density filtering was chosen so that the average intensity of the reference beam was roughly the same as the average intensity of the object beam at the same exposure time; the initial ND filter was used to avoid excessive saturation at the CCD. The filtering varied depending on the object used for reconstruction. For each holographic reconstruction, we captured two beam profiles: the profile of the combined beam and, by blocking the object beam, the one from the reference beam only. The reason why the reference beam was needed is that holographic reconstruction is performed by reading off the differences in phases between corresponding points of the reference and object beams. The reference beam provides a "background" for comparison.

Immediately after expansion of the laser beam, we obtained two types of intensity profile: an airy disk and a Gaussian. (See Figure 3.) An airy disk intensity profile was undesirable because its black fringes, corresponding to destructive interference of light from diffraction, are areas where no information of the object could be retrieved for reconstruction; this is because no light would be reflected off the object at the fringes. The Gaussian profile was desirable because it is smooth, lacking points of destructive interference. Of course, a perfect Gaussian was not possible to achieve, and so dark fringes from an approximately smooth Gaussian were cut off by passing the expanded laser beam through an iris.

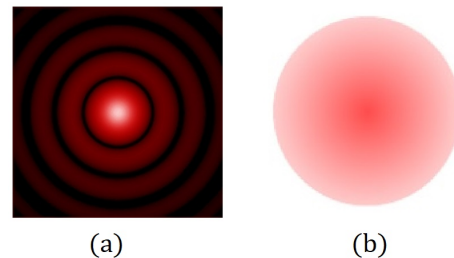


FIG. 3: (a) Airy disk intensity profile.[8] (b) Gaussian intensity profile.[7]

By far, the most important part of the experimental setup was the alignment of the laser beam. A good enough method for aligning the laser is to close the iris to allow the minimum amount of light to pass through it, then ensure that the light at each obstacle (beam splitters, mirror, object, camera) position hits a mounted target (we used a target printed on a safety card), so that the laser point at each obstacle position was centered and at the same height.

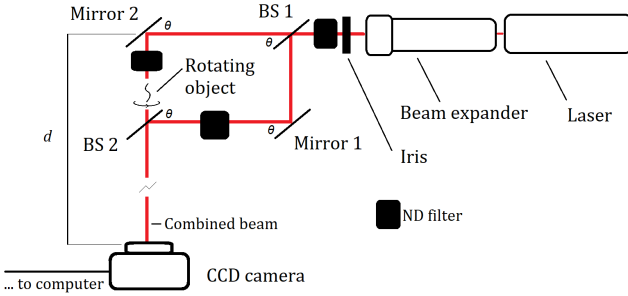


FIG. 4: Setup for tomographic reconstructions.  $d = 0.33\text{m}$ ;  $\theta = 45^\circ$ .

For the setup for tomographic reconstructions, it was necessary to replace the object in Figure 2 by a second mirror. (See Figure 4.) Alignment of the object beam reflected off the new mirror and the reference beam was performed by closing the iris and overlapping the two points, one from each beam, captured by the CCD camera (the other obstacles were already aligned from the previous setup). (See Figure 5.) A rotating object was placed in between the second mirror and the second beam splitter. ND filters served the same purposes as for the setup for 2D holographic reconstructions.

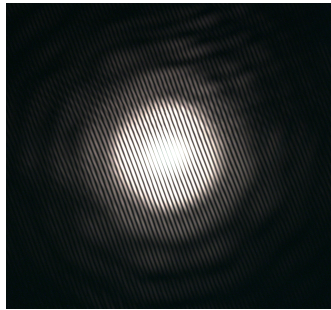


FIG. 5: Beam alignment for tomography setup: as seen on the computer when iris was closed as much as possible, the points from the reference beam and object beam are superimposed. A poor alignment would show two distinguishable points.

The method used for tomographic reconstructions was a 13-angle reconstruction method. Thirteen captures of the combined beam, one for each different angle of rotation of the object, were taken; the steps were of  $15^\circ$  between 0 and  $180^\circ$ . The rotation of the object was achieved with a servo motor controlled by an Arduino board. A capture of only the reference beam profile was also taken; the purpose of this becomes clear in the Results and analysis section.

The computer program used for numerical reconstructions was MATLAB. All reconstructions were performed based on code borrowed from Nehmetallah, et. al. (2015).

#### IV. RESULTS AND ANALYSIS

##### A. 2D holographic reconstruction

The field at the CCD camera is given by  $h(x, y)$  in Equation 3.  $h(x, y)$  contains the complete information (irradiance and

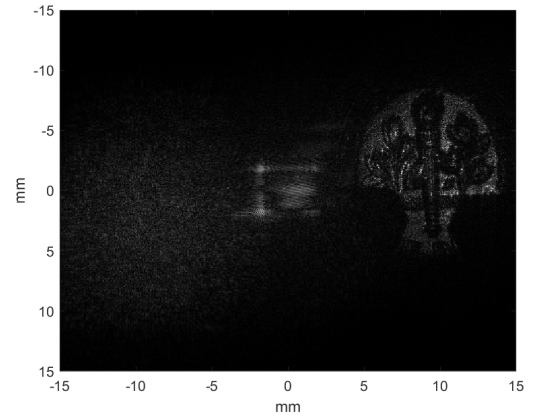


FIG. 6: Complete reconstruction of the information contained in the function  $h(x, y)$  in Equation (3). From left to right: virtual image, DC term, real image. Parameters:  $d = 0.45\text{m}$ , initial filtering: ND OD 1.7; for matching intensities of reference and object beams: reference beam filtering: ND OD 2.6.

phases) of the points of both the object and reference beams [3]:

$$h(x, y) = [|E_O|^2 + |E_R|^2] + E_O E_R^* + E_O^* E_R, \quad (4)$$

where  $E_O$  is the field of the object beam at the CCD, and  $E_R$  is the field at the CCD of the reference beam. Figure 6 shows a holographic reconstruction of a US dime. Relating Figure 6 and the function  $h(x, y)$ , the first term in the brackets to the right of  $h(x, y)$  contains information about the DC term, which is the bright square at the center of the reconstruction in Figure 6 (this term is considered noisy and its effects on the reconstruction are reduced by subtracting the average irradiance off the beam profiles; this is called “DC term subtraction”) the second term contains information about the virtual image, which is the blurred image to the left of the figure; the third term contains information about the real image, which is the reconstruction to the right.

Notice that the field of the reference beam is multiplying the complex conjugate of the object beam in Equation (4); this distorts the real image,[6] because the phase of the reference beam alters that of the object beam. This is corrected by multiplying  $h(x, y)$  by the complex conjugate of the reference beam; the term containing information of the real image becomes:

$$E_O^* |E_R|^2. \quad (5)$$

This correction is inserted into Equation 3:

$$\begin{aligned} \Gamma(\xi, \eta) &= \frac{i}{\lambda} \exp(-i \frac{2\pi}{\lambda} d) \exp(-i\pi\lambda d[(\frac{m}{N\Delta x})^2 + (\frac{n}{N\Delta y})^2]) \\ &\times \sum_{k=0}^{N-1} \sum_{l=0}^{N-1} h(x, y) E_R^* \exp(-i \frac{pi}{\lambda d} [(k\Delta x)^2 + (l\Delta y)^2]) \\ &\exp(i2\pi(\frac{km}{N} + \frac{ln}{N})), \\ m &= 0, 1, 2, \dots, N-1; n = 0, 1, 2, \dots, N-1, \end{aligned} \quad (6)$$

The term  $E_R^*$  in Equation (6) is controversial; it is obtained from the reference beam profile *alone*, with the object beam blocked. How could a complex conjugate be extracted out of the information about the reference beam profile, which is

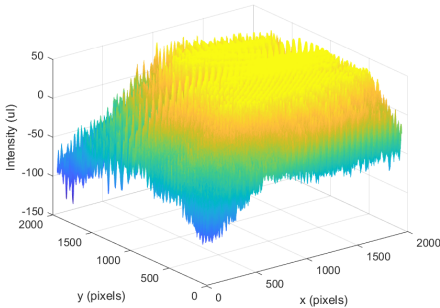


FIG. 7: 3D graph of the profile of the reference beam used in the reconstruction of the US dime in figures 6 and 8 (a).

just a bunch of *real* numbers, recorded by the CCD? I cannot see a way to thi this, and I think it is impossible to do. A fix for this is to consider the reference beam to be a plane wave. If the reference beam has a planar front, then we can approximate  $E_R$  to be constant; since, for reconstruction, the interest lies on the differences between the phases of the object beam and the reference beam of corresponding points, the phase of the object beam can be defined up to a constant (this constant been the phase of the planar reference beam) and we can set this constant to equal zero. This forces the field of the reference beam to be real. So, for the plane wave approximation:

$$E_R \approx E_R^* = \text{constant} \in \Re. \quad (7)$$

The reconstructions shown in figures 6 and 8 (a), which are the same, were performed using the plane wave approximation of the reference beam. The average irradiance of the beams was subtracted from  $h(x, y)$  to reduce the effects of the DC term to obtain a better resolution; also,  $E_R$  was rescaled accordingly by making it fluctuate around zero. Then, it was assumed that  $E_R \approx E_R^* \approx 40.723\text{uI}$  after DC term subtraction, which is, approximately, the average value of the maximum points of intensity in the beam profile (it corresponds to a range 199 to 255uI before DC term subtraction)(uI is just a unit of intensity; the computer just reads numbers). The CCD camera was saturated just enough for this (the reason why this could be valid becomes clear in the Discussion section). Figure 7 shows the three-dimensional intensity profile of the reference beam used for the reconstruction of the US dime in figures 6 and 8 (a).

The other available option is to consider the fluctuations in the phases of the points of the reference beam at the CCD to be small enough with respect to a zero phase; this is to be able to approximate the reference beam to be real. This time, however, the field of the reference beam at the CCD would be a (real) function of  $x$  and  $y$ , since the wave front is not taken to be completely planar:

$$E_R \approx E_R^* \approx f(x, y) \in \Re. \quad (8)$$

For this, we use the reference beam profile captured by the CCD and insert it directly into Equation 6. Figure 8 compares the reconstructions of a US dime for the plane wave approximation and for the (real)  $f(x, y)$  approximation. The results are better for the plane wave approximation.

It was found that for two objects that have similar reflective properties, the quality of the reconstruction depends on

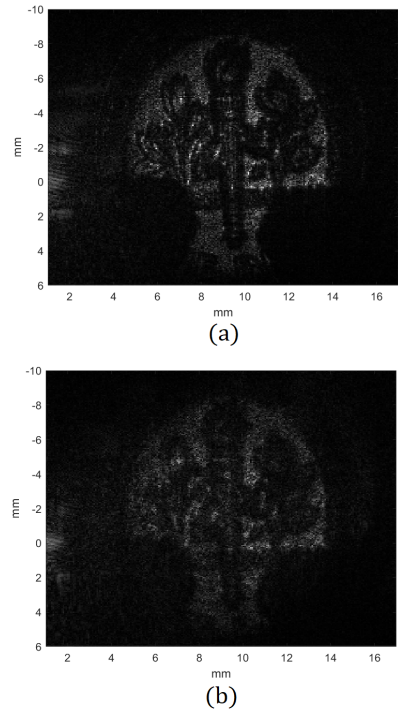


FIG. 8: US dime reconstruction: (a) plane wave approximation of reference beam,  $E_R \approx E_R^* \approx 40.723\text{uI}$ ; (b) approximation of reference beam to real function  $E_R \approx E_R^* \approx f(x, y) \in \Re$ . Parameters:  $d = 0.45\text{m}$ , initial filtering: ND OD 1.7; for matching intensities of reference and object beams: reference beam filtering: ND OD 2.6.

the complexity of the high relief pattern. The more complex the high relief, the better the reconstruction. The reason for this can be traced back to the idea that digital holographic reconstruction is based on reading off differences in phases of corresponding points in the object and reference beam profiles. Figure 9 shows the reconstruction of a CAD dime using the plane wave approximation of the reference beam  $E_R \approx E_R^* \approx 32\text{uI}$  after DC term subtraction (255uI before DC term subtraction). The CAD dime is mostly flat, and so the computer has difficulty reading off phase differences except at the points where the high relief is notably pronounced, such as the contour of the queen's head. Compare this figure to the reconstruction of the US dime in Figure 8 (a).

## B. Tomographic reconstruction

Two three-dimensional reconstructions were attempted. Figures 10 (c) & (d) and 11 (c) show the attempts at reconstructing the wire and cylinder in Figure 10 (a) and the wire loop in Figure 11 (a), respectively. The respective combined beams (or “shadows”) are shown in figures 10 (b) and 11 (b). The tomographic reconstruction in Figure 10 was performed using the plane wave approximation, and the reconstruction in Figure 11 was performed using the approximation of the reference beam to a real function  $f(x, y)$ .

Evidently, the tomographic reconstructions were not *completely* successful. Nevertheless, the fact that, in Figure 10, a cylindrical geometry was reproduced successfully and that,

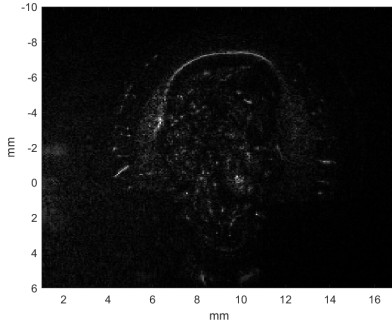


FIG. 9: Reconstruction of a CAD dime using the plane wave approximation for the reference beam:  $E_R \approx E_R^* \approx 32\text{uJ}$ . Parameters:  $d = 0.45\text{m}$ , initial filtering: ND OD 2.1; for matching intensities of reference and object beams: reference beam filtering: ND OD 2.3.

in Figure 11, a “hole” in the reconstruction is seen, which suggests that the computer attempted to reconstructed the arc in the wire loop, indicates that we are not chasing ghosts. The achievement of a completely successful tomographic reconstruction could be a matter of tweaking the setup and improving the method employed for capturing beam profiles.

Figure 10 shows two tomographic reconstructions for two reasons: the real distance between the CCD object was  $0.33\text{m}$ ; setting the parameter for this distance in the computer to be  $d = 0.33\text{m}$  generates the poor reconstruction shown in Figure 10 (d); in contrast, setting  $d = 0.09\text{m}$ , in the computer, even when the real distance was  $0.33\text{m}$ , gives the better reconstruction of Figure 10 (a). One of the reasons that could be contributing to the unsuccessful tomographic reconstructions may have to do with the saturation of the CCD. Figure 12 shows the intensity profiles of the reference beam and the shadow used for the reconstruction of the wire and cylinder in Figure 10. The CCD was over-saturated, with nearly all points hitting the maximum of 42 units of intensity after DC term subtraction; for this capture,  $42\text{uJ}$  corresponded to the maximum of  $255\text{uJ}$  that the CCD can read before DC subtraction. This could be the reason why setting a false distance parameter gave a better reconstruction: the phases of the reference and object beam could have been distorted by the oversaturation, making the computer think that the object was closer to the CCD than it really was.

Non-saturation of the CCD, however seems to be undesirable all the same. Figure 13 (a) shows the intensity profile of the reference beam used for the reconstruction of the wire loop in Figure 11. it is evident that the reference beam profile as captured by the CCD is far away from the plane wave approximation; it looks more like a Gaussian. This meant that there were spots of low intensity in the combined beam profile, as shown in Figure 13 (b), the 3D intensity of profile of the shadow in Figure 11 (b). The computer may be thinking that those low-irradiance spots correspond to shadows of a non-existing object and it may be trying to reconstruct them. The question here is: would *just enough* saturation of the CCD be a key factor for successful holographic reconstructions in general?

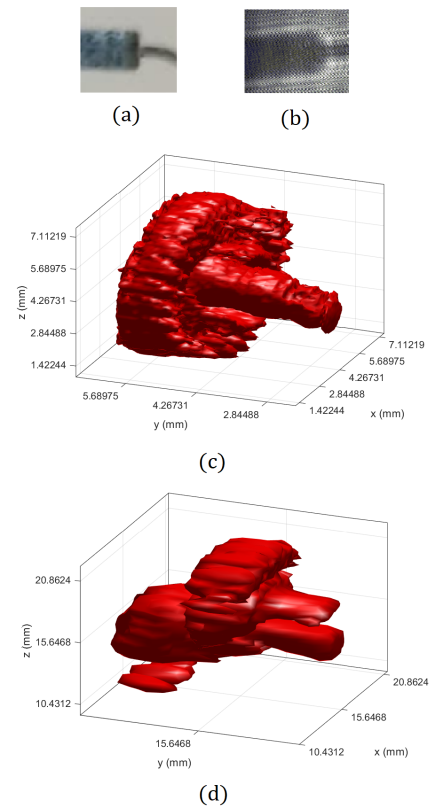


FIG. 10: (a) Wire and cylinder as object for reconstruction. (b) Combined beam: shadow of the object when hit by the laser light reflected off mirror 2 in Figure 4. (c) Attempt at tomographic reconstruction with fake distance parameter  $d = 0.09\text{m}$ . (d) Attempt at reconstruction using real distance  $d = 0.33\text{m}$  as parameter. Real parameters:  $d = 0.33\text{m}$ ; filtering unknown, but intensities of object and reference beam were matched. The dimensions of the reconstruction are 1000 times the real ones.

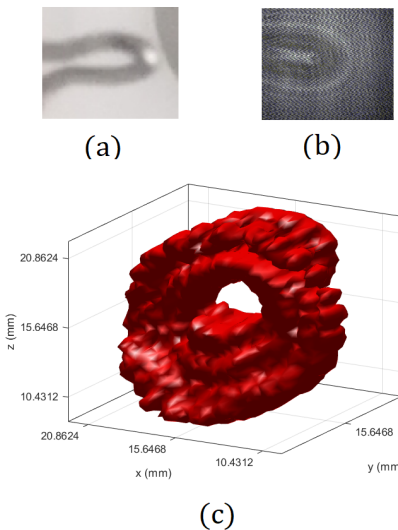


FIG. 11: (a) Wire loop as object for reconstruction. (b) Combined beam: shadow of the object when hit by the laser light reflected off mirror 2 in Figure 4. (c) Attempt at tomographic reconstruction. Real parameters:  $d = 0.33\text{m}$ , initial filtering: ND OD 3.0; for matching intensities of object and reference beams: object beam filtering: ND OD 1.3, reference beam filtering: 1.4. The dimensions of the reconstruction are 1000 times the real ones.

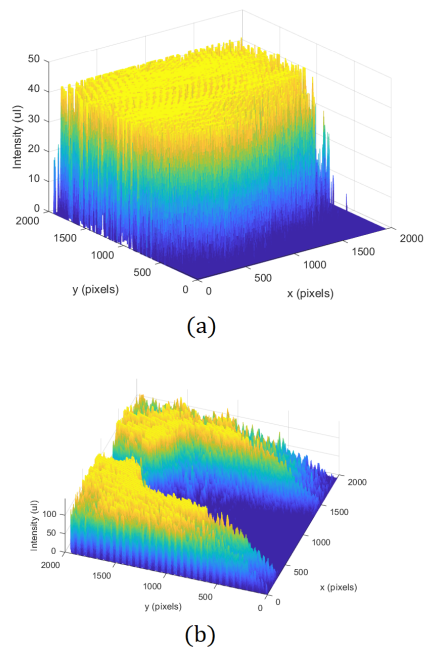


FIG. 12: Beam profiles used for the reconstructions in Figure 10: (a) reference beam intensity profile; (b) combined beam intensity profile.

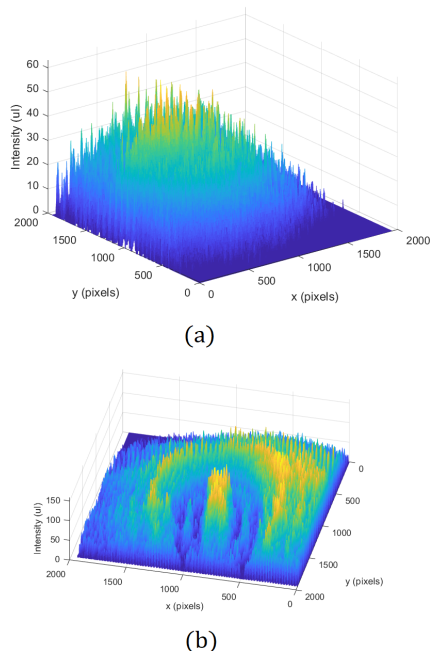


FIG. 13: Beam profiles used for the reconstructions in Figure 11 (a) reference beam intensity profile; (b) combined beam intensity profile.

## V. DISCUSSION

The results of this experiment indicate that, although the essential information for holographic reconstruction is in the phases of the beams, the irradiance profiles of the beams at the CCD play an important role as well, specially in tomographic reconstructions. The intensity profiles of the beams at the CCD seem to play a role of “preservation of phases”.

Saturation of the CCD occurs at intensity values above 255uJ before DC term subtraction. For 2D reconstructions: the reference beam used for reconstruction of the US dime (Figure 8), the largest intensity values at the CCD are in the range of 199-255uJ before DC term subtraction. Although the CCD was saturated at some points, just enough saturation was necessary for the employment of the plane wave approximation discussed in the Results and analysis section. The reconstruction of the US dime can be considered successful. For the CAD dime (Figure 9), most of the largest intensity values of the reference beam used for its reconstruction were all at 255uJ, so saturation definitely occurred. We cannot be sure how bad the saturation was above this point, but we could evaluate the level of saturation by judging the quality of a holographic reconstruction. For the CAD dime, however, this is hard to do because its surface was mostly flat. We noted, from several attempts that varied in exposure time and filtering at reconstructing surfaces with overall flat patterns, that the results could not get better, and this was the case for the CAD dime. One of the explanations for this could be that phase information dominated over irradiance information. For a mostly flat surface, the phases of the object beam would be more or less equal, and so the computer would read something flat, which shows as a dark spot in the reconstruction. A better way to look at this is by imagining reconstructing a circular mirror. The computer will read an

irradiance pattern from the CCD, but it will not see any differences in the phases of the points reflected off the mirror. The computer would only read the edge of the mirror, where a contrast in phase values is seen, and the reconstruction would look something like a bright circular ring and everything dark inside it. This is exactly what happened with the CAD dime; the most noticeable features of the queen are the contour of her head, where the computer could clearly see a contrast in phases between the head of the queen and the background of the coin. Also notice that the flat background in the US dime was not reconstructed either, further supporting the idea that contrast in phases reflected off a surface are crucial for better 2D holographic reconstructions.

Things complicate when we take a look at the tomographic reconstructions. The observations made on phase and irradiance influence on 2D reconstructions could be non-definitive whatsoever. First, we look at the intensity profiles in Figure 12, corresponding to the tomographic reconstructions of the wire and cylinder in Figure 10. The largest intensities of the reference beam read by the CCD are all at 255 uJ before DC term subtraction. The saturation is evident as it is evident that the reconstruction of the wire and cylinder is very poor with a distance parameter  $d = 0.33\text{m}$  (the actual real distance between the CCD and the object). Nonetheless, the reconstruction at a fake distance (parameter)  $d = 0.09\text{m}$  is much better. Could oversaturation of the CCD have distorted the phases of the object beam in the term containing its information:  $E_O^*|E_R|^2$  (Equation (5))? It could be that the amplitudes of the object beam,  $|E_O|$ , and of the reference beam,  $|E_R|$ , were much larger than the complex factor in  $E_O^*$ , making the computer think that the object was closer than it appeared. But non-saturation seems to be as detrimental for reconstruction as oversaturation is. Figure 13 shows the intensity profiles corresponding to the reconstruction of the wire loop in Figure 11. The intensity profile of the reference beam is more like a Gaussian, and a plane wave approximation is inappropriate. This time, without saturation of the CCD, some of the features of the wire loop can be seen in its reconstruction at the correct distance parameter  $d = 0.33\text{m}$ ; for example, the hole in the reconstruction could correspond to the arc in the loop. This suggests that, indeed, oversaturation distorts the phase reading done by the computer, altering the computer's perception of distance between the CCD and the object. Nevertheless, the reconstruction of the wire loop cannot be considered successful: the reconstruction looks more like a doughnut than an arc. The reason for this could be that there was no saturation of the CCD. In the intensity profile of the shadow of the wire loop in Figure 13 (b), we can see other zones of low intensity apart from the shadow of the object. The computer could be interpreting those as shadows cast from non-existing objects and it might be that it is incorporating all this into the reconstruction, closing the loop to form a doughnut.

Another factor contributing to poor tomographic reconstructions in general could be not-good-enough alignment of the laser. Although the technique used for alignment for the setup for tomographic reconstructions guarantees that both the object beam and the reference beam hit the camera at the same spot, as shown in Figure 5, some underlying factor in alignment, such as possibly not having had the beams being completely perpendicular to the CCD pixel grid plane

and the object being too thick, may be contributing to the poor reconstructions. If the beam is not completely normal to the pixel grid, for example, the computer would be looking at an oval-shaped cross-section of the beam rather than at a circular cross-section for a perpendicular beam.

The observations made above seem to indicate a correlation between the goodness of the plane wave approximation with the goodness of the holographic reconstruction. A good plane wave approximation could be obtained by saturating the camera just enough so that the complex factor in the term containing information about the real image for reconstruction,  $E_O^*|E_R|^2$ , is not much smaller than the intensities of the beams. A systematic method of obtaining this kind of saturation could be forcing the object and reference beams to each have exactly maximum intensity values *just over* half 255uJ, so that when they combine (these form the combined beam), the CCD would be saturated just enough that the phases are not negligible. Meanwhile, the  $E_R^*$  term in  $E_O^*|E_R|^2$  would come from a new capture of the intensity profile of the reference beam only, and it would be such that its maximum intensity values are *just over* 255uJ; this way, we can perform the plane wave approximation on the reference beam only without overshadowing the complex term in  $E_O^*|E_R|^2$ . In the laboratory, my partner and I tried to do something similar, but we made the mistake of measuring the average intensities of the object and reference beam instead of their maximum values. At the same time, the larger the contrast in phases contained in the object beam part in the combined beam, the better. In the case of a 2D reconstruction, a dispersive reflection off the object's surface is desirable, and the more complex its high relief structure is, the better. Further exploration on holography could be the extraction of information about depths of a surface, and that could possibly be done more easily by performing a 3D reconstruction of the surface using a tomographic reconstruction method.

## VI. CONCLUSIONS

The quality of the two-dimensional holographic reconstruction of a surface depends on the complexity of its high relief pattern and on the saturation level of the CCD camera used to record its hologram. With an appropriate saturation of the CCD, the more complex the high relief structure of the surface, the better the reconstruction. By an appropriate saturation of the CCD, one can refer to one in which the maximum intensities of the points of the wavefront hitting, and as recorded by, the CCD are just above the maximum value of intensity that the CCD can read. This is to be applied to every intensity profile recorded by the CCD in order to be able to approximate the reference beam as a plane wave without distorting the phase information about the object's surface contained in the object beam. The plane wave approximation gives the best results for 2D holographic reconstructions, and it is speculated that the case is the same for tomographic reconstructions, although conclusions for the latter are not definitive. Other factors, like a meticulous laser alignment and the thickness of the object to be reconstructed, are expected to have an impact on the quality of the tomography.

- 
- [1] Kreis, T. (2012). Applications of Digital Holography: From Microscopy to 3D-Television. Journal of the European Optical Society - Rapid publications, Europe, v. 7, mar. 2012. ISSN 1990-2573.  
Retrieved from: [http://www.jeos.org/index.php/jeos\\_rp/article/view/12006](http://www.jeos.org/index.php/jeos_rp/article/view/12006). Date accessed: 15 April, 2019. doi:314.
- [2] Micó, V & Ferreira, Cassius & Zalevsky, Zeev & García-Monreal, Javier. (2019). Basic principles and applications of digital holographic microscopy.  
Retrieved from: [https://www.researchgate.net/publication/266067304\\_Basic\\_principles\\_and\\_applications\\_of\\_digital\\_holographic\\_microscopy](https://www.researchgate.net/publication/266067304_Basic_principles_and_applications_of_digital_holographic_microscopy). Date accessed: 14 April, 2019.
- [3] Nehmetallah, G.; Rola, A.; Williams, L. (2015). *Analog and digital holography with MATLAB*. USA: SPIE. P. 52.
- [4] Osten, Wolfgang & Faridian, Ahmad & Gao, Peng & Körner, Klaus & Naik, Dinesh & Pedrini, Giancarlo & Singh, Alok Kumar & Takeda, Mitsuo & Wilke, Marc. (2014). Recent advances in digital holography [Invited]. Applied Optics. 53. 10.1364/AO.53.000G44.  
Retrieved from: [https://www.researchgate.net/publication/264352804\\_Recent\\_advances\\_in\\_digital\\_holography](https://www.researchgate.net/publication/264352804_Recent_advances_in_digital_holography).
- Invited. Date accessed: 14 April, 2019.
- [5] Pedrotti, Frank L.; Pedrotti, Leno M.; Pedrotti, Leno S. (2017). *Introduction to optics*. USA: Cambridge University Press.  
Pp. 469-470.
- [6] Schnars, U. & Jueptner, W. (2005). *Digital holography. Digital hologram recording, numerical reconstruction, and related techniques*. Germany: Springer.  
P. 15; p. 16; p. 47; p. 46; p. 23.
- [7] Laser gaussian profile. Retrieved on April 8th, 2019 from: [https://commons.wikimedia.org/wiki/File:Laser\\_gaussian\\_profile.svg](https://commons.wikimedia.org/wiki/File:Laser_gaussian_profile.svg).
- [8] Diffraction. Retrieved on April 8th, 2019 from: <https://simple.wikipedia.org/wiki/Diffraction#/media/File:Airy-pattern2.jpg>.

## NOTES

- [9] Theory heavily borrowed from Schnars & Jueptner (2005), chapters 2 and 3.